Journal of Molecular Catalysis A: Chemical 332 (2010) 93–105

Contents lists available at ScienceDirect

Journal of Molecular Catalysis A: Chemical

journal homepage: www.elsevier.com/locate/molcata

Various characteristics and catalytic performance of iron (II) phthalocyanine immobilized onto titania- and vanadia-pillared bentonite clay in *in situ* polymerization of methyl methacrylate
An attempt to synthesize novel polymer/iron phthalocyanine/pillared clay nanocomposites

Salah A. Hassan[a,*], Fatma Z. Yehia[b], Hamdi A. Hassan[a], Salwa A. Sadek[a], Atef S. Darwish[a]

[a] Department of Chemistry, Faculty of Science, Ain Shams University, Abbassia, Cairo, Egypt
[b] Department of Petrochemicals, Egyptian Petroleum Research Institute, Nasr City, Cairo, Egypt

ARTICLE INFO

Article history:
Received 19 June 2010
Received in revised form 1 September 2010
Accepted 1 September 2010
Available online 16 September 2010

Keywords:
Titania-pillared bentonite
Vanadia-pillared bentonite
Iron (II) phthalocyanine
In situ polymerization
PMMA/FePc/pillared bentonite nanocomposites

ABSTRACT

Pure bentonite clay has been modified through acid thermal treatment (ATTB) and by pillaring with titania and vanadia (Ti-PILB and V-PILB). Iron (II) phthalocyanine complex (FePc) was immobilized in 0.5 wt% loading on the modified bentonite supports. Structural characteristics were investigated through XRD, FTIR and ICP-EDX techniques. Textural and morphological characteristics were estimated from adsorption–desorption isotherms of N_2, pore size distribution analysis and SEM. Dispersion parameters of FePc molecules were determined from H_2 chemisorption isotherms at 300 °C. Cation exchange capacities and acid–base behaviours were also studied. Incorporation of oriented FePc was found to reorganize the clay layer stacking, being deformed upon modification, through interaction with pillar (in V-PILB) or with interlayer sites (in Ti-PILB). Catalytic performance of different samples in *in situ* bulk polymerization of methyl methacrylate at 60 °C was discussed, where living polymerization mechanism, within the role of FePc in re-initiation of dormant polymer molecules, was confirmed. $\overline{M}_w$ and $\overline{M}_n$ of produced polymers decreased, according to the used support, in the order: Ti-PILB > ATTB > V-PILB, the same decreasing order of chain transfer constant (C_T), related to contribution of FePc. A new approach for synthesis of polymer/modified bentonite composites of partially exfoliated layers was provided. In PMMA/FePc/V-PILB composite, nanoclay particles (of 25 nm) were shown with more ordered polymer chains and well dispersed vanadia pillar species, in a strong interaction and high compatibility with FePc.

© 2010 Elsevier B.V. All rights reserved.

1. Introduction

Several transition metal complexes, such as metal phthalocyanines (MPc) and metal porphyrins (MP) have been applied widely in the last two decades in a variety of polymerization reactions (e.g., [1–4]). For stabilizing such metallomacrocycles against possible deactivating dimerization and destructive processes, immobilization on a suitable solid matrix was applied to add some benefits from steric and electronic effects of the support [1,3,5–7]. Among the known matrices used are synthetic and natural clays, especially of montmorillonite group. They are widely applied as supports as well as catalysts in many reactions, e.g., alkylation [8], isomerization [9] and polymerization [10–12]. They are also recently involved in synthesis of composites with particular thermo-mechanical and electrical properties [12–15]. Different polymerizations, such as suspension, emulsion and *in situ* bulk polymerization were used for synthesis of a number of polymer–clay composites [13–16].

Since the efficient use of clays as catalysts was limited by the lack of porosity and low thermal stability, several modifications were proposed, e.g., by intercalating the clay with large polyoxocations as well as with macrocyclic metal complexes [17,18]. Pillaring consists in converting the layered clay into highly porous structure by exchanging the compensating interlayer cations with a variety of inorganic polyoxocations. Upon heat treatment, such poly-cationic species are transformed into rigid pillars, linking permanently the silicate sheets, and forming two-dimensional zeolite-like materials, known as pillared interlayered clays (PILCs). Titania- and vanadia- pillared clays have received less attention than the other oxide- pillared ones, due probably to the preparation difficulties. Ti-PILCs have been explored as catalysts in many applications, e.g., dehydration [19], cracking and hydrocracking [20], photo-catalytic degradation [21], alkylation [22], oxidation [23] and selective

* Corresponding author. Tel.: +20 2 37494856; fax: +20 2 24831836.
E-mail address: salahabdo40@yahoo.com (S.A. Hassan).

1381-1169/$ – see front matter © 2010 Elsevier B.V. All rights reserved.
doi:10.1016/j.molcata.2010.09.004

catalytic reduction (SCR) of NO [24]. With regards to V-PILCs, much fewer papers could be found, concerning with their preparation, characterization and application as catalysts [25–27].

Transition metal complexes supported on such silicate structures, e.g., bentonite, have gained special interest with regards to their marked reactivity and selectivity in various processes [3,7,28–31]. During the immobilization of charged complexes, solvent and matrix cooperative effects were suggested arising from both the clay interlayer environment and the clay surface of special catalytic interest [30]. Only very limited works have dealt with intercalated complexes into pillared clays interlayers, where both pillars and intercalates were expected to involve in the catalytic applications [29,32,33].

Amongst the scarce researches to the application of metal complexes/montmorillonite clay systems in heterogeneous polymerization of olefins, appeared our guide work [3] to explore the functionality of supported Ni (II) and Cu (II) phthalocynines (NiPc and CuPc) of 0.2–2.2 wt% loadings/Indian bentonite in bulk polymerization of methyl methacrylate (MMA) at 80 °C, using $NaHSO_3$ cocatalyst. For loadings ≥1.0 wt%, redox radical initiation–propagation steps were confirmed, contributed from ionic mechanism characteristic of pure unmodified bentonite. The reaction proceeded in much lower yields or even ceased in absence of HSO_3^-. Recently, role of anchorage mode of the same NiPc and CuPc complexes, of an optimum 1.8 wt% loading, to bentonite surface in controlling catalytic performances in early stage of the polymerization process, in aqueous and emulsion media, was studied in the temperature range, 40–60 °C [18]. Redox-free radical mechanisms suggested dual-site initiation in presence of NiPc molecules, intercalated into bentonite clay galleries parallel to silicate layer planes. Single-site initiation by using CuPc system was linked with inclined edge-on orientation of the complex molecules, leading to facile access of Cu sites to MMA monomer and HSO_3^- cocatalyst from both sides.

Inspection of literature, however, has detected that insufficient attention has been paid to the behaviour of supported phthalocyanine complexes on modified clays, e.g., pillared bentonite, in polymerization of MMA. Complexities that have to arise from various interactions involving the complex, the pillars and the clay interlayer sites have not been approached.

The present work was thus undertaken to characterize the modified bentonite, viz., through acid thermal treatment (ATTB) and by pillaring with titania and vanadia (Ti-PILB and V-PILB), as well as the hybrid catalytic system of Fe (II) phthalocyanine (FePc) immobilized onto modified clay samples (in 0.5 wt%, of diluted loading region). Catalytic performance of these systems in the *in situ* polymerization of MMA was followed up at 60 °C, in absence of a cocatalyst, aiming to elucidate the competing roles played by the complex, the pillars and the interlayer sites in the reaction mechanism, compared with other phthalocyanine systems. The study was extended to use the obtained results in an attempt to synthesize novel PMMA/FePc (compatibilizer)/pillared clay (filler) nanocomposites, as polymerization end products.

2. Experimental

2.1. Modification of bentonite clay

Pure potassium and calcium-rich bentonite clay (PROLABO) had the following composition (mass%): O, 56.99; Si, 32.98; Al, 4.47; Mg, 0.44; Fe, 1.83; Ca, 1.46 and K, 1.83. Acid-thermal activation of parent raw bentonite (RB) was carried out by soaking it in a 6 M HCl solution (solid/liquid ratio = 1:15) for 18 h at 70 °C. After discarding the acid and washing with deionized water until pH = 6, the separated clay slurry was dried at 100 °C for 18 h and calcined at 300 °C for 4 h. This treated bentonite was designated as ATTB. For preparation of titania-pillared bentonite (Ti-PILB), the pillaring solution was first obtained by slow dissolution of an appropriate amount of $TiCl_4$ in 6 M HCl with vigorous stirring, adjusting final concentrations by dilution to be 0.09 M in Ti and 1 M in HCl (i.e., $H^+/Ti = 1:11$). The fresh pillaring solution was then added drop wise to 500 cm^3 of a suspension containing 30 g of ATTB, such that the final Ti/clay ratio was 0.60 mmol g^{-1} [17,22]. The product was filtered, washed with distilled water, dried gradually and then calcined at 300 °C for 4 h in a flow of dry air. Vanadia-pillared bentonite (V-PILB) was prepared by refluxing $VOCl_3$/dry toluene pillaring solution of an appropriate concentration together with pre-weighed pure bentonite sample, under N_2 atmosphere, until the clay suspension turned green in color [25]. A final V/clay ratio of 1.0 mmol g^{-1} was achieved. The product was filtered, washed with dry toluene to remove excess of $VOCl_3$ then dried and calcined as for Ti-PILB.

2.2. Preparation of immobilized complex samples

Iron (II) phthalocyanine (FePc) was synthesized according to [34], applying some modification described elsewhere [7]. The complex was immobilized onto different modified bentonite supports in a 0.5 wt% loading, i.e., not exceeding 10% of the monolayer formation. A pre-weighed clay sample was impregnated with the appropriate quantity of FePc in 100 ml of 4 M H_2SO_4 with continuous stirring for 12 h at room temperature. The produced catalyst sample was filtered, washed thoroughly with distilled water, dried for 12 h at 100 °C and calcined for 4 h at 260 °C in atmospheric air.

2.3. Characterization of different samples

Physicochemical characterization of RB, ATTB, Ti-PILB and V-PILB as well as the immobilized complex samples was performed using the conventional techniques, viz., XRD with a Phillips model PW3710-BASED diffractometer operated at 40 kV and 55 mA using Ni-filtered CuKα radiation (λ = 1.5418 Å) and FTIR with ATi Mattson, WI, 53717 model Genesis spectrometer, USA, with a nominal resolution of 2 cm^{-1}. Chemical analyses were carried out through energy dispersive X-ray spectroscopy (EDXS), on JEOL JSM-840 A, Oxford model 16211, with a resolution of 1.3 eV and diffraction traces taken in RIGAKU D/MAX-C instrument using CuKα radiation (λ = 1.5405 Å), and inductively coupled plasma (ICP-OES) on a JY-24 instrument, performing sample digestion in an Anton Paar multi-wave instrument. Cation exchange capacities (CEC, in mequiv./100 g) were estimated by the aid of copper bisethylenediamine complex $[Cu(en)_2]^{2+}$ method [35] and changes in surface acid–base properties were followed up potentiometrically [36], adopting some recently described models [37].

The texture of various samples was investigated via BET surface area determination and pore size analysis, based on adsorption–desorption isotherms of N_2 at −196 °C [38]. Their morphology was studied through scanning electron microscopy (SEM) on a JEOL JSM-5400 working at 30 kV. The sample surface was sputter-coated with gold for 3 min. TEM of some samples was also performed on JEOL 1200 EX II, at 120 kV with resolution of 0.2 nm.

The degree of dispersion of the immobilized FePc was determined from H_2 chemisorption isotherms, measured at 300 °C in a micro-volumetric apparatus up to $P_{eq} \sim 250$ Torr (1 Torr = 1.33×10^2 Pa), following the same lines of previous discussions [6,28]. The so-called "net adsorption uptakes" (n_{H_2}, in mmol H_2 g^{-1} sample), calculated from the isotherms by correction for pure supports, were used to estimate the degree of complex dispersion (D) as the ratio of n_{H2} or equivalently number of surface complex molecules [n_{FePc}]: total number of complex molecules in the sample. Surface areas of the complex (S_{FePc}, in m^2 $g^{-1}{}_{FePc}$) and

stoichiometries of H_2 adsorption were determined to assess the orientation models, according to [6,7,18].

2.4. In situ polymerization of methyl methacrylate (MMA)

In a typical *in situ* polymerization experiment, freshly distilled stabilizer-free monomer was introduced into the reaction tube together with the catalyst sample, concentration of which was 3.56% (w/w), with respect to the monomer [3,10]. The tube was sealed under N_2 atmosphere and placed in a thermostat adjusted at 60 °C for different time intervals, between 0.5 and 24 h. At the assigned time interval, the tube was carefully opened and the content was dissolved in appropriate amount of chloroform under occasional shaking. After filtration to remove the catalyst and the unconverted monomer, the free polymer was precipitated from concentrated solution by running into methanol (10 ml of alcohol for each 1 ml of the polymer solution). The produced polymer was washed and dried under vacuum at 40 °C till constant weight. The polymer yield or % monomer conversion (Y, %) was calculated as:

$$Y\,(\%) = \frac{\text{weight of the produced polymer}}{\text{initial weight of monomer}} \times 100.$$

The same procedure was used to obtain a polymer/clay composite, without separating the hybrid complex–catalyst system at the end of the polymerization process.

2.5. Characterization of polymethyl methacrylate (PMMA) samples

PMMA samples produced were characterized by determining its number-average molecular weight ($\overline{M}_n$), weight-average molecular weight ($\overline{M}_w$) and polydispersity index ($\overline{M}_w/\overline{M}_n$) via gel permeation chromatography (GPC). The high pressure GPC consisted of a high pressure pump (type 600E multi-solvent delivery system), four ultra styragel HR chromatographic columns of 7.8 mm, I.D. 300 mm, connected in series and a differential refractometer (type M 2410) as the detector. The measurements were carried out in toluene of HPLC grade as a mobile phase with a rate of elution, 0.7 ml min^{-1} at 40 °C. The molecular weights were determined relative to mono disperse polystyrene standards [3]. Stereotacticity of polymers was determined from ^{1}HNMR spectra using a JEOL EX-270 MHz spectrometer with superconducting magnet and 5 mm Dual probe head. Spectral width, data points and flip angle were 4000 Hz, 32 K and 45°, respectively. $CDCl_3$ was used as a solvent and tetramethyl silane as an internal reference.

3. Results and discussion

3.1. Physicochemical characteristics of modified bentonite and immobilized complex samples

3.1.1. XRD analysis

The XRD patterns, in the low angle range, of the parent bentonite clay (RB) and its modified samples, viz., ATTB, Ti-PILB and V-PILB, are shown in Fig. 1(a). Basal (0 0 1) d-spacing, full width at half maximum peak height (FWHM) of basal d(0 0 1) and relative intensities of most characteristic peaks are given in Table 1. For RB, the 2θ of basal (0 0 1) reflection at 5.75° corresponds to d-spacing of 15.34 Å, linked with the presence of Ca- and Na-rich montmorillonite as dominant clay mineral, with smaller amount of illite [39]. The two-dimensional (hk) reflections at 2θ = 19.79° (summation of (0 2) and (1 1) indices), arise from diffraction of random stacking of the layers and the peak at 2θ of 21.8° indicates the reflection of (1 0 1) plane of OCT (opal-CT, paracrystalline silica). The low value of FWHM of the basal d(0 0 1) points to high stacking order of TOT elementary layers in the clay [40].

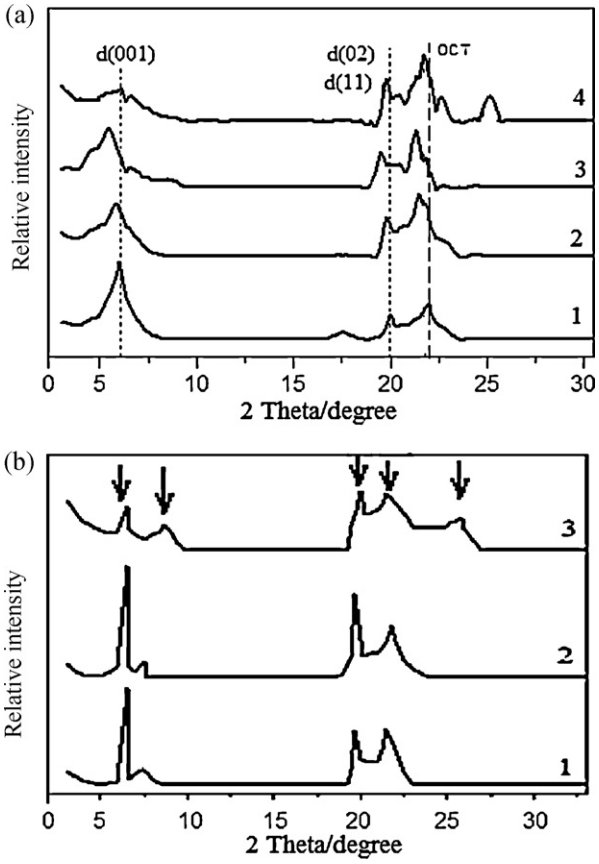

Fig. 1. XRD patterns of: (a) neat modified bentonite supports: (1) RB, (2) ATTB, (3) V-PILB, (4) Ti-PILB, and (b) immobilized FePc onto: (1) ATTB, (2) V-PILB and (3) Ti-PILB.

For ATTB sample, some decrease in the intensity of basal d(0 0 1) diffraction peak, although 2θ of parent bentonite is preserved, may refer to deposition of paracrystalline silica, resulted from the acid attack on the octahedral layer, exposing the tetrahedral layer [41]. Consequently, the intensity of OCT increases from 31% in RB to 100% in ATTB (Table 1). The marked increase in d(0 0 1) FWHM value and the significant increase in the intensity of (0 2) and (1 1) peak at 2θ of 19.69°, from 19% in RB to 53% in ATTB, reveal enhanced disorder of layer stacking beside dealumination or delamination of the clay galleries [42].

In V-PILB, the basal (0 0 1) peak is shown to shift slightly to lower 2θ (viz., 5.39°) (Fig. 1(a)), corresponding to some expansion of the basal spacing from 15.34 Å in RB to 16.42 Å in V-PILB. Vanadia pillar seems to locate just beneath the edge surface, i.e., expanding the edges of the clay sheets. This intense and sharp peak with larger FWHM value, of 0.16° (Table 1), ensures a disturbance in the original layer arrangement, although overall crystalline structure of the clay is almost preserved. The absence of crystalline V_2O_3 or V_2O_5

Table 1
XRD parameters of most characteristic peaks for parent and modified bentonite supports and different immobilized FePc samples.

Samples	d_{001} (Å)	I_{001} (%)	FWHM$_{001}$ (°)	$I_{02\&11}$ (%)	I_{101} (%)
RB	15.34	100	0.06	19	31
ATTB	15.22	60	0.40	53	100
V-PILB	16.42	100	0.16	66	89
Ti-PILB	15.28	16	0.32	55	100
FePc/ATTB	13.64	100	0.08	24	44
FePc/VPILB	13.58	100	0.08	64	30
FePc/TiPILB	13.48	37	0.06	57	94

characteristic peaks may be attributed to the presence of dispersed nano-sized or isolated tetrahedral species, in the interlayers. The marked increase in intensity of (0 2) and (1 1) reflections of TOT (Table 1), compared to RB, confirms the possible deformation in layer arrangements. Higher intensity of (1 0 1) peak of OCT points to dealumination or delamination as other causes of the deformation.

The XRD pattern of Ti-PILB (Fig. 1(a)) shows a broader (0 0 1) band of lower intensity (16%) at $2\theta = 5.78^\circ$ of FWHM = 0.32° (Table 1), indicating a decline in the clay crystallinity with lower ordering in layer stacking [41]. It was previously reported for poorly crystalline Ti-PILC [24] that (0 0 1) reflections are hardly observed. However, appearance of a weak peak at 25.7° (25%), characteristic of anatase, ensures the presence of extra-lattice titania in the clay interlayers [42], being susceptible to agglomerate and intercalate as oligomeric polyoxocations. The average size of anatase particles was found to be 88 nm, as calculated through Scherer equation [43], based on the corresponding FWHM value. Intercalation of titania pillar leads to a significant lowering in the intensity of (0 0 1) basal line and a lack of ordering in c-direction, as a result of dealumination [42]. Marked increases in intensities of (0 2) and (1 1) and OCT (1 0 1) peaks reflect marked diminish of layer stacking and more pronounced deformation.

It is clearly evident for the immobilized FePc (0.5 wt%) onto different modified bentonite supports (ATTB, V-PILB and Ti-PILB) that, incorporation of the complex into clay galleries causes reorganization of the layers with more stacking order (Fig. 1(b)). In view of the shift of (0 0 1) diffraction peak to little higher 2θ values ($\sim 6.5^\circ$), an increase in its intensity, (especially in ATTB and V-PILB), some decrease in d(0 0 1) spacing and a marked decrease in FWHM value (Table 1), the intercalated complex may be considered as binding the basal planes. This may result from different interactions facing the complex with pillars and/or interlayer sites. The sharp decrease in intensity of (1 0 1) peak of OCT suggests the involvement of tetrahedral sheets and edge sites in the interactions. On the other hand, the weak characteristic peaks of FePc, appeared at $2\theta = 7.6^\circ$ (3%) in V-PILB and ATTB or 9.1° (18%) in Ti-PILB, may be related to the complex location at layer edges, anchored probably in an oriented profile.

3.1.2. FTIR analysis

From FTIR spectrum of the parent bentonite, RB (Fig. 2(a)), montmorillonite is shown to be the dominant mineral phase; the absorption bands at 908 cm^{-1} and at 836 cm^{-1} confirm the presence of dioctahedral smectite with AlAl–OH, AlFe–OH and AlMg–OH bending vibrations [44]. The absorption bands in the 1000–1200 cm^{-1} region reflect stretching vibrations of Si–O groups in the silicate structure, viz., asymmetric stretching vibrations of apical oxygens of SiO_2 tetrahedra and combined stretching and bending vibrations of Si–O bonds related to basal oxygens [45]. The bands at 514 and 465 cm^{-1} are due to Al–O–Si (Al in octahedral sheet) and Si–O–Si bending vibrations, respectively [41]. The band at 620 cm^{-1} is assigned to coupled Al–O and Si–O out-of-plane vibrations, while that one at 784 cm^{-1} corresponds to disordered OCT [39]. The effect of acid thermal activation can be observed via elimination of AlAl–OH, AlFe–OH and AlMg–OH bending bands around 908 cm^{-1} and of Al–O–Si bending band at 514 cm^{-1}, with an appearance of more significant band of coupled Al–O and Si–O out-of-plane vibrations at 620 cm^{-1} and of paracrystalline silica (OCT) at 784 cm^{-1}, confirming structural deformation of the octahedral sheet structure [46]. The intensities of Si–O–Si in-plane stretching bands in the region, 1000–1200 cm^{-1} and of Si–O–Si bending band at 467 cm^{-1} remained unaffected by the acid treatment, pointing to preservation of the whole layer structure.

The spectrum of V-PILB (Fig. 2(a)) has all absorption bands characteristic of amorphous silica (OCT), particularly at 788 cm^{-1}, revealing structural deformation of the clay galleries. Here, elimination of the band at 908 cm^{-1} (of AlAl–OH bending) points to probable interaction of vanadia with some layer edge sites. The spectrum shows also V=O stretching vibrations of isolated VO_x species at 1010 cm^{-1}, V–O–V vibrational modes involving vanadia at 760 cm^{-1}, as a result of the mentioned interactions [47]. The absence of 994 cm^{-1} and 697 cm^{-1} bands ensures that no or only a few of nano-sized V_2O_5 crystals were formed during the calcination. For Ti-PILB, the weakened band at 780 cm^{-1} of amorphous silica and the new one at 979 cm^{-1}, of Ti–O–Ti, can be attributed to the location of titanium polyoxocations deeply in the clay interlayers, probably in some weaker electrostatic interaction with silica tetrahedral sheets. No bands characteristic of Ti–O–Si and Ti=O, related to strong covalent interaction, could be seen.

The FTIR spectra of the FePc immobilized on ATTB, V-PILB and Ti-PILB (Fig. 2(b)) reveal strong masking effect of the supports used.

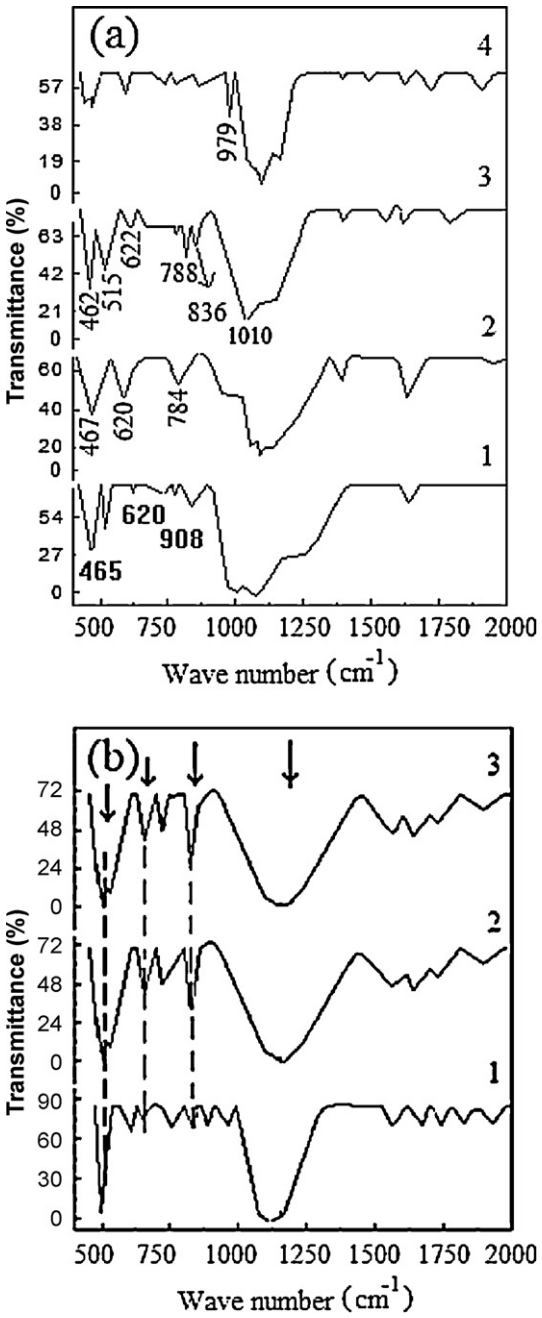

Fig. 2. FTIR spectra of: (a) parent and modified bentonite supports: (1) RB, (2) ATTB, (3) V-PILB, (4) Ti-PILB and (b) immobilized FePc onto: (1) ATTB, (2) V-PILB and (3) Ti-PILB.

Table 2
Main data derived from EDX and ICP analyses, cation exchange capacities, PZNPC and surface charge site densities for various samples under study.

Samples	M^a (μmol g^{-1})	Si/Al[b]	X_{Fe}	X_v or X_{Ti}	CEC (meq/100 g)	PZNPC	Surface charge site densities (sites nm^{-2})		
							D_{SiO^-}	D_{AlOH}	D_{CE}
RB	589	6.7	–	–	66.9	10.14	452	163	290
ATTB	380	9.2	–	–	62.0	8.46	177	139	154
V-PILB	425	7.1	–	0.9	25.0	6.97	3291	1970	233
Ti-PILB	466	6.7	–	2.0	55.0	8.88	93	63	128
FePc/ATTB	356	6.4	1.0	–	101.7	5.59	236	144	287
FePc/V-PILB	430	6.6	1.1	0.8	137.3	5.09	1200	581	1236
FePc/Ti-PILB	406	7.2	1.4	1.8	92.7	4.15	1355	922	508

[a] Content of exchangeable cations calculated by ICP.
[b] Estimated from EDX and ICP analyses.

As strong and broad bands in the 940–1260 cm^{-1} region, assigned to Si–O–Si vibrations [45], are overlapping with the most characteristic bands of FePc, one cannot exclude the involvement of Si-tetrahedral sheets in the interaction of the complex with different interlayer sites of the modified bentonite supports.

3.1.3. Chemical analysis

The results derived from chemical analyses by EDX and ICP (Table 2) reveal that, the acid activation of bentonite has led to a significant increase in Si/Al ratio (from 6.7 to 9.2), due to dealumination in the octahedral sheet with considerable leaching of exchangeable cations (cf., M contents in μmol g^{-1} clay by ICP), especially Ca^{2+} and Mg^{2+} reaching to 0.0%. Reduction in the amount of exchangeable cations upon pillaring with titania and vanadia reflects the successful insertion of pillar species into the clay interlayers. Incorporation of FePc into the ATTB interlayers causes some sort of reorganization of TOT elementary layers, where Si/Al ratio has regained its original value of RB (≈6.7). However, incorporation of FePc into V-PILB structure cannot show a clear involvement of exchangeable cations, due probably to aggregation of V-species near the layer edges. Upon immobilizing FePc onto Ti-PILB, the large decrease in the amount of exchangeable cations points to more interaction of the complex with various exchange sites in the interlayers, nearly without affecting the original Si/Al ratio.

To better represent the mode of aggregation of V, Ti and FePc species, incorporated in the studied systems, an aggregation factor (X) was calculated as the ratio of the concentration assumed theoretically for preparation (in μmol g^{-1} sample), based on the monomeric model of the concerned species, to that actually found from ICP analysis. The aggregation factors of vanadia (X_v) in V-PILB and of titania (X_{Ti}) in Ti-PILB are shown to be nearly equal to 1 and 2, respectively (Table 2). This may suggest that, vanadia locates as single isolated tetrahedral species near the layer edges, while titania is inserted in some flocculated form, probably deeply in the clay interlayers. In all cases, the immobilized FePc seems to exist as separate monomeric molecules (X_{Fe} = ∼1), most probably in an oriented profile [7].

3.1.4. Acid–base characteristics and cation exchange capacities

Changes in surface acid–base properties of bentonite, after modification and by anchoring the FePc complex, were followed up potentiometrically [36], applying the recently reported three-site model [37]. According to this model, amphoteric aluminol, acidic silanol and basic basal plane cation exchange site densities, i.e., D_{AlOH}, D_{SiO^-} and D_{CE} (sites nm^{-2}), respectively, were calculated. Based on the titration curves, D_{AlOH}, was derived from the number of edge aluminol surface charges ($\sigma_{H\ edge}$) and D_{SiO^-} was derived from the number of silica surface charges in edge planes, ($\sigma_{o^-\ edge}$), while D_{CE} was derived from the number of basal proton surface charges, $\sigma_{H\ basal}$ [48]. Cation exchange capacity (CEC), determined according to [35], point of zero net proton charge (PZNPC) [37,48] and calculated surface charge densities for the studied samples are included in Table 2.

It is evident from Table 2 that, parent bentonite exhibits a quite high CEC characterizing the TOT structure [44]. For ATTB, the decrease in CEC and the loss of about half of the original basal CE site density (D_{CE}), reveal effective elimination of a great deal of exchangeable cations in the clay octahedral sheet. The shift of PZNPC to more acidity, (from 10.14 to 8.46), can be linked with the protons trapped in the clay interlayers. Reduction in D_{AlOH}, D_{SiO^-}, confirms both dealumination and delamination of the clay structure.

For V-PILB, the marked decrease in CEC illustrates accumulation of vanadia species at the edges, impeding the action of most of the interlayer exchangeable cations; their site density remains only slightly affected. The shift of PZNPC to more surface acidity may be referred to obvious acidity of VO_x species beside evolution of silanols, resulting from strong interaction with Si–O–Si and its breaking [27] (cf. FTIR data). Due to presence of vanadia near the layer edges, exposing the edge aluminols and silanols, both D_{AlOH} and D_{SiO^-} are markedly increased (Table 2). For Ti-PILB, the decrease in CEC and the marked depression in D_{CE} may ensure the deeper intercalation of titania agglomerates in the clay interlayers. Strong deformation of layer structure assists occupation of most of silanol and aluminol sites at the edges and deeply in the interlayers (cf., loss of D_{AlOH} and D_{SiO^-}). This leads to more surface acidity, where protons intercalation seems to accompany the Ti-pillar insertion.

By incorporating FePc into modified bentonite supports under study, the surface acid–base behaviours seem to be strongly affected, in terms of the increase in CEC and corresponding surface charge densities, compared with the neat supports (Table 2). The change in CEC is associated with changes in Lewis acidity arising from structural defects, broken bonds and hydroxyl transfers [35]. For FePc/ATTB, a marked increase in D_{CE} may refer to the attack of Al–O–Mg and/or Al–O–Fe, in the octahedral sheet, after leaching out the exchangeable extra lattice cations. This is linked with a shift of PZNPC toward more acidic value. For FePc/V-PILB, it appears most likely that, the immobilized FePc interacts with V-polyoxocations at the edge sites, encouraging their dissociation into isolated tetrahedral vanadia species, of higher Lewis acidity (lower PZNPC). The complex–vanadia interaction seems to impede other interactions of vanadia with interlayer sites, regaining Si–O–Si and Al–O–Al bridges, as emphasized by lower silanol and aluminol site densities compared with the neat support. For FePc/Ti-PILB, the complex seems to interact with interlayer sites, involving tetrahedral silica, and edge sites, involving octahedral alumina, rather than with titania pillar species (cf., marked increase in D_{SiO^-} and D_{AlOH} and observed lowering in PZNPC). In all supports, the complex interactions with the pillar or with the interlayer sites may encourage creation of new active exchange sites.

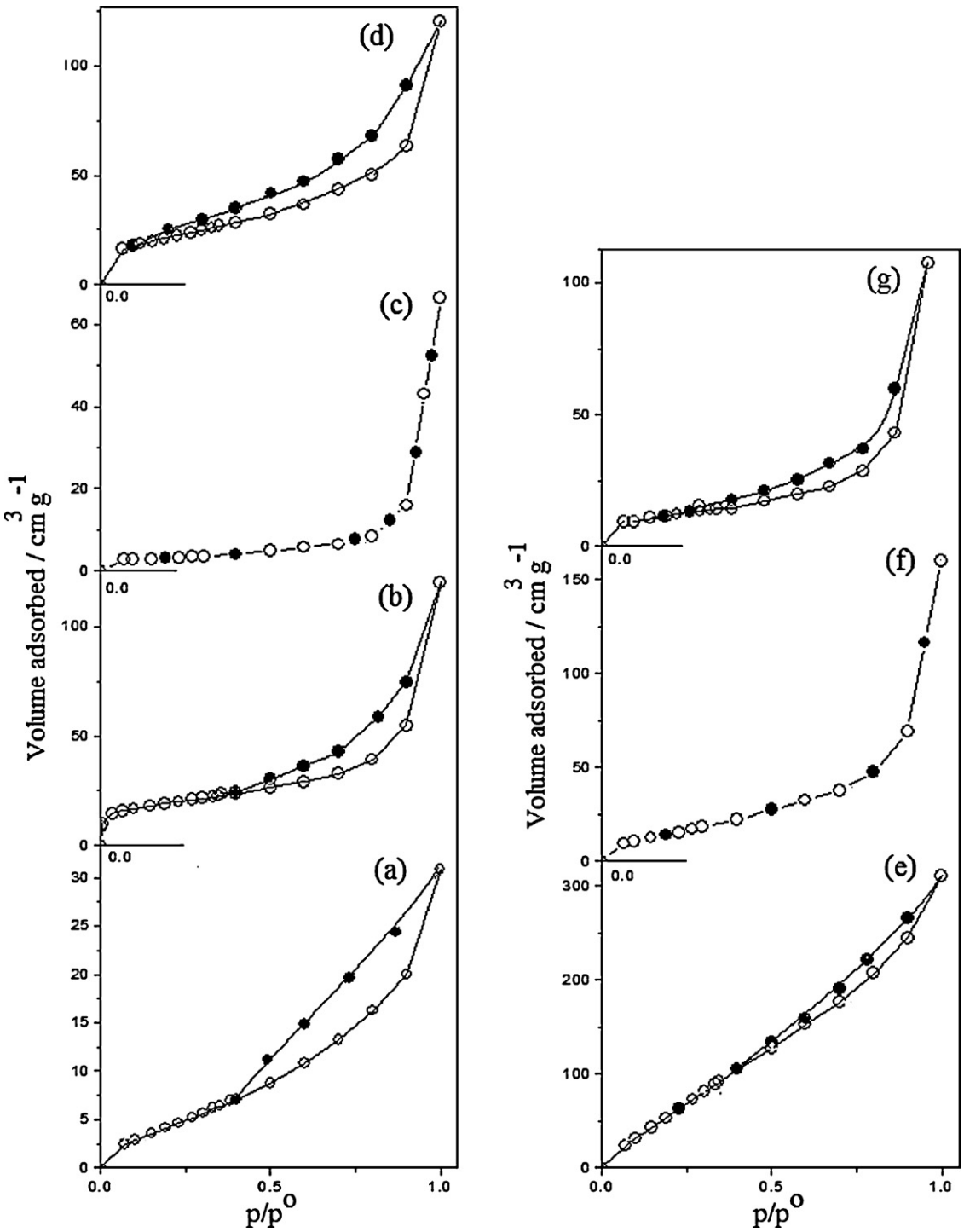

Fig. 3. N_2 adsorption–desorption isotherms at −196 °C on: (a) RB, (b) ATTB, (c) V-PILB, (d) Ti-PILB, (e) FePc/ATTB, (f) FePc/V-PILB and (g) FePc/Ti-PILB.

Table 3
Surface characteristics of neat supports and immobilized complex samples, and dispersion parameters of immobilized FePc complex derived from H_2-chemisorption data.

Samples	S_{BET} ($m^2\ g^{-1}$)	$V_p^{0.95}$ ($ml\ g^{-1}$)	r_h^{pp} (nm)	S_t ($m^2\ g^{-1}$)	$r^{pp}_{most\ abund}$ (nm)[a]	H_2 ads. stoich. (n_{H2}/n_{Fe}^{2+})	S_{FePc} ($m^2\ g^{-1}{}_{FePc}$)	$[D]_{app}$
RB	20.38	0.0480	4.73	25.67	0.92–1.16			
ATTB	65.68	0.1866	5.68	58.29	0.92–1.86			
V-PILB	10.76	0.1034	19.22	11.90	1.21–3.00			
Ti-PILB	78.41	0.1871	4.77	74.44	1.83			
FePc/ATTB	65.69	0.1866	5.68	59.64	1.85	2.19 (2:1)	59.1	0.768
FePc/V-PILB	37.14	0.2604	14.02	51.14	1.43	2.40 (2:1)	49.0	0.699
FePc/Ti-PILB	40.23	0.1667	8.29	39.26	1.88– 3.80	1.97 (2:1)	165.7	0.522

[a] Most abundant approximate pore radius derived from PSD curves.

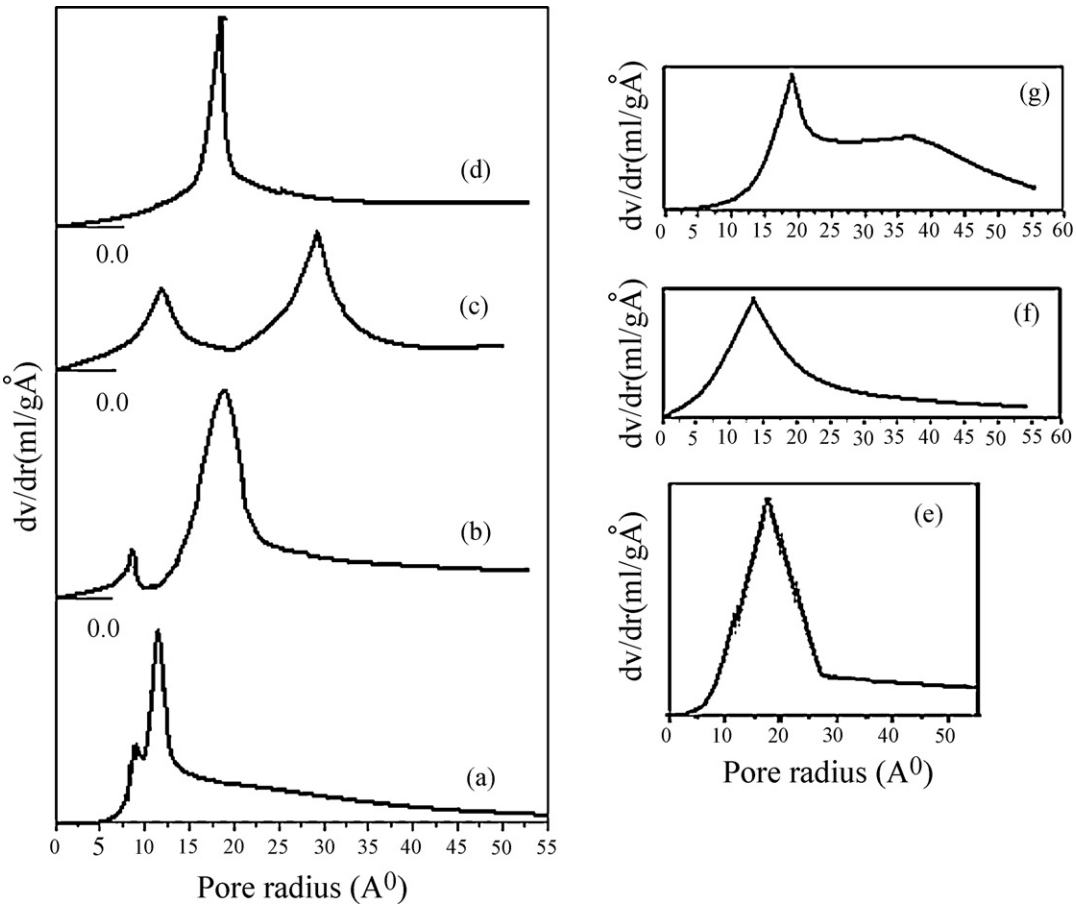

Fig. 4. Pore size distribution curves for: (a) RB, (b) ATTB, (c) V-PILB, (d) Ti-PILB, (e) FePc/ATTB, (f) FePc/V-PILB and (g) FePc/Ti-PILB.

3.2. Textural and morphological investigation of different samples under study

The obtained adsorption–desorption isotherms of N_2 at −196 °C on the surface of the parent and modified bentonite supports as well as the immobilized FePc samples are illustrated in Fig. 3, being almost of type II in the classification of Sing et al. [38]. The closed hysteresis loops in the case of ATTB and Ti-PILB are of type H3, which characterizes aggregates of plate-like particles giving rise to slit-shaped pores [38]. For V-PILB, the completely reversible isotherm may be linked with evolution of larger fraction of mesoporosity. Immobilization of Fepc did not change markedly the shapes of the obtained isotherms on neat supports. The derived surface parameters are given in Table 3 including specific surface areas (S_{BET}, $m^2\,g^{-1}$), pore volumes (V_p, $ml\,g^{-1}$) estimated at 0.95 p/p_o and average pore radii ($\bar{r}_p^{pp}$) assuming parallel plate (pp) pore model. For ATTB and Ti-PILB, the evident increase in surface area and total pore volume seems to be related to deformation of octahedral sheet structure from leaching of some exchangeable cations. V-PILB exhibits lower surface area, with an increase in pore mouth dimensions, reflecting accumulation of a fraction of vanadia pillar probably at layer edges.

For further investigation of the existing pore systems, pore size distribution (PSD) curves for various samples are depicted in Fig. 4. For RB, a larger fraction of micropores of most frequent hydraulic radius of ~12 Å is shown beside a smaller fraction of most frequent radius of ~9 Å (Table 3). This represents the thickness of TOT layer, as the turbostatic stacking of elementary layers in clay tactoids creates slit-shaped micropores on broken edges of the layers [49]. For ATTB, acid treatment leads to an increase in the radius of the larger fraction of pores to 18.6 Å, whereas for Ti-PILB, intercalation of agglomerated titania pillar into clay interlayers eliminates a number of micro-sized pores. For V-PILB, bimodal pore system reveals creation of a fraction of larger mesopores of most hydraulic radius of 30 Å, confirming the accumulation of V-pillar at layer edges. In general, the micropores fraction of 9 Å is clearly eliminated by insertion of the complex or the pillars in clay layer structure. For FePc/V-PILB, elimination of larger fraction of 30 Å may result from the interaction between FePc and vanadia particles. For FePc/Ti-PILB, deeper intercalation of FePc in the interlayers may create a fraction of wider pores.

The morphology of various samples examined via SEM is illustrated in Fig. 5. The ATTB and Ti-PILB samples, in micrographs (a and b), show irregular and looser curved flakes, indicating structural deformation and disordered stacking of clay layers, due to dealumination (etching). Insertion of flocculated titania pillar seems to leave large voids. Clay layered structure associated with mats of coalesced flakes is clear for V-PILB (micrograph c); vanadia probably accumulates at some edges in a dispersed manner. The micrographs (d and e) of immobilized FePc onto ATTB and Ti-PILB confirm more etching by intercalated complex molecules together with some ordering of clay layer stacking. However, for FePc/V-PILB, micrograph (f) reveals smaller clay flakes with more randomly arranged layers, due almost to strong interaction of FePc molecules with vanadia pillar, causing its dissociation at clay edges. Confirming this interaction, TEM investigation of neat V-PILB support and immobilized FePc/V-PILB sample (Fig. 6) shows that larger vanadia particles, originally present in the modified clay (of size

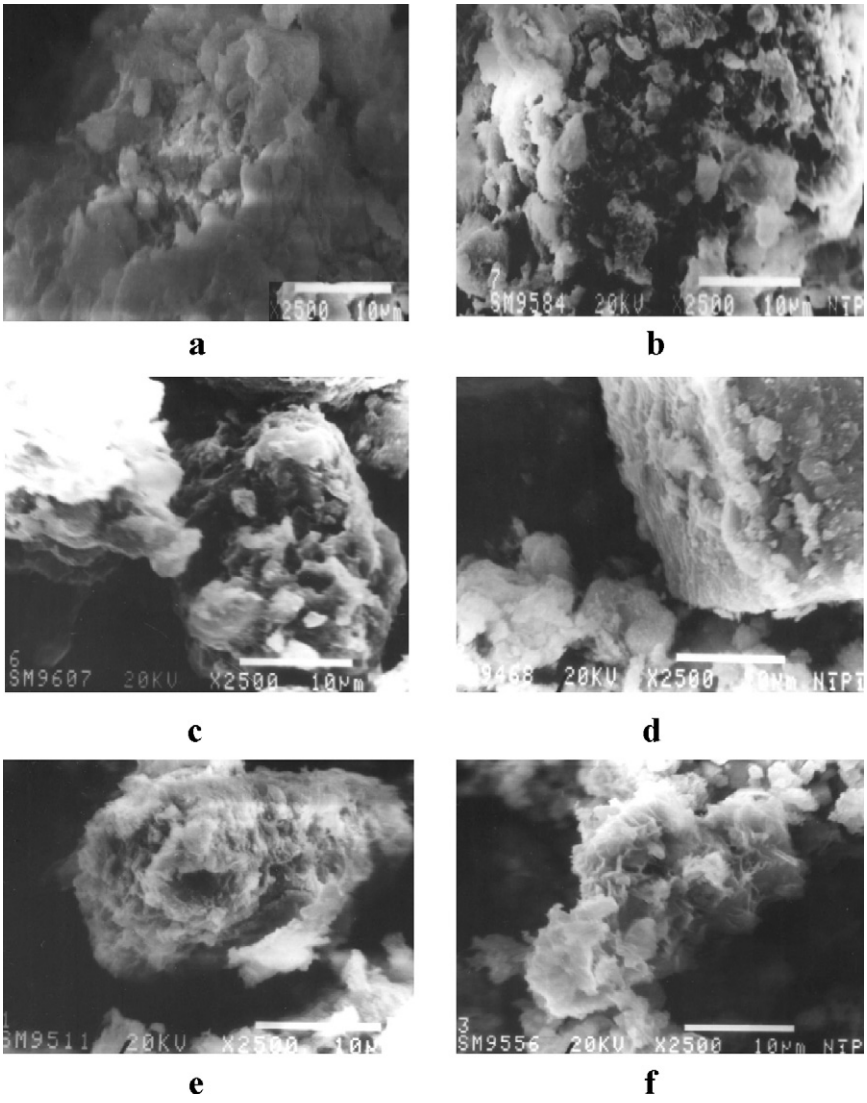

Fig. 5. Scanning electron micrographs of: (a) ATTB, (b) Ti-PILB, (c) V-PILB, (d) FePc/ATTB, (e) FePc/Ti-PILB and (f) FePc/V-PILB.

ranged between 27 and 163 nm), has been dissociated into dispersed smaller particles (of 12–19 nm) in the immobilized sample. Such system, involving strong interaction between oriented complex molecules and vanadia polyoxocations in the pillared clay layer structure, can be considered as promising catalytic nanohybrid composite, to be adopted in several applications.

3.3. Surface dispersion and orientation characteristics of the immobilized FeP complex

The mode of orientation of FePc molecules could be assessed by the aid of H_2-chemisorption isotherms at 300 °C through determining the adsorption stoichiometry ($n_{H_2}/n_{Fe^{2+}}$) according to [6,18,28].

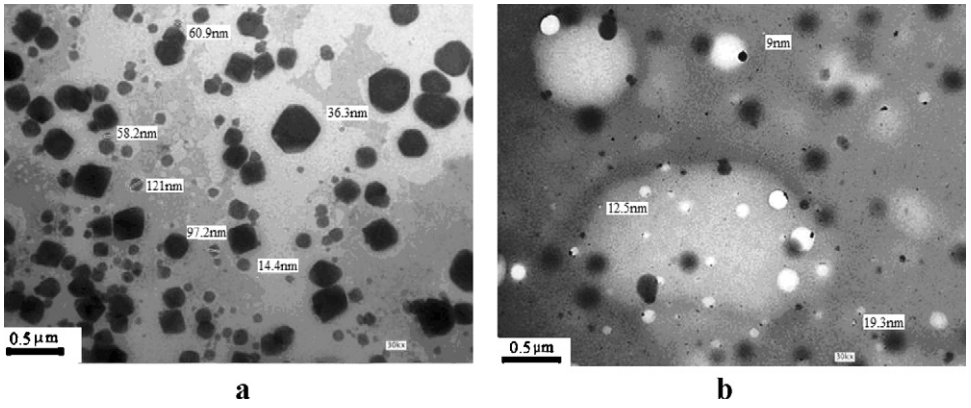

Fig. 6. Transmission electron micrographs of: (a) V-PILB and (b) FePc immobilized onto V-PILB.

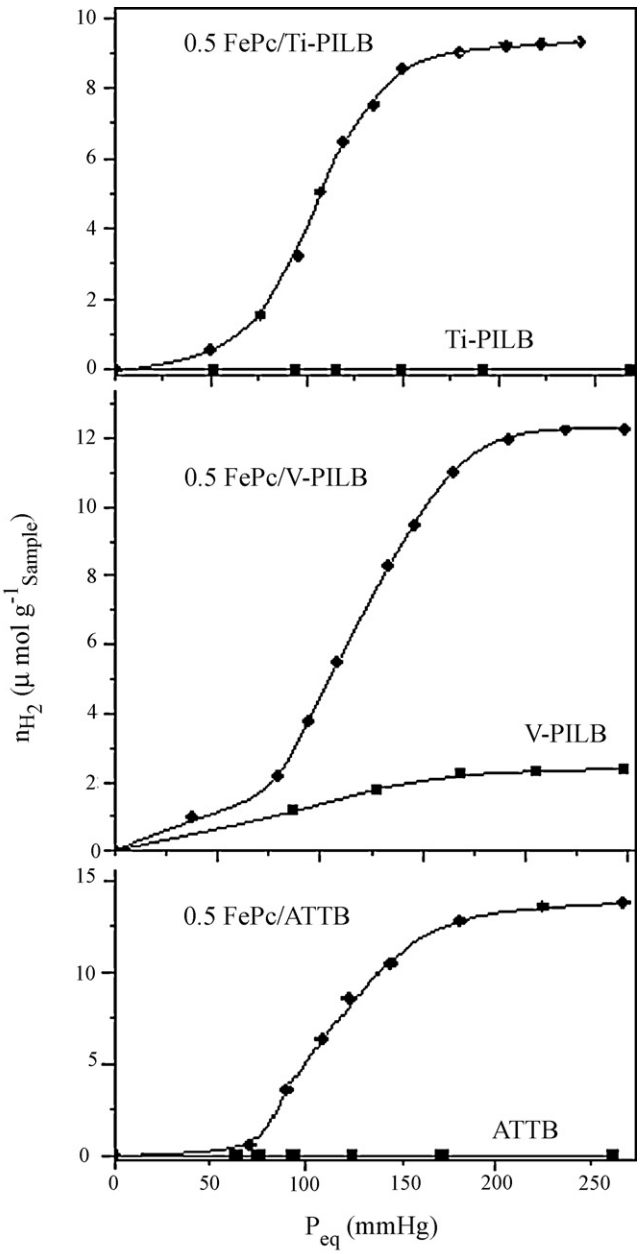

Fig. 7. Chemisorption isotherms of H_2 at 300 °C on: ATTB, V-PILB and Ti-PILB and the corresponding immobilized FePc (0.5 wt%) catalyst samples.

The isotherms obtained show almost monolayer coverage (Fig. 7); only small or undetectable H_2 uptakes could be measured on neat modified bentonite supports up to ~250 Torr, while immobilized FePc samples recorded much higher uptakes, referring to their highly dispersed nature. It is evident from Table 3, that calculated stoichiometry of H_2-adsorption on all immobilized FePc samples is close to 2:1, implying that H_2 is axially ligated to vacant d-orbitals of the central Fe ion from both sides. This should be favored most probably by inclined edge-on interaction between *N*'s of the macro-ring system and edge OH sites of the clay, via asymmetric Brønsted interaction [6,7,18], behaving similar to CuPc on pure unmodified bentonite [18]. The inclined edge-on orientation of FePc molecules at the edge surface or inside the clay layers may be accepted in view of the clay basal spacing, being >1.5 nm (Table 1), compared with the complex height of the order ~1.1 nm [18,28]. Such mode of orientation, accompanied with higher degrees of dispersion $[D]_{app}$ and higher metallic surface areas (S_{FePc}) (Table 3), allows facile accessibility of FePc molecules to several interactions, e.g., complex–complex, complex–pillar and complex–interlayer sites.

3.4. Catalytic performance of investigated samples in in situ polymerization of MMA

Fig. 8 illustrates typical kinetic curves of *in situ* bulk polymerization of MMA at 60 °C, in presence of different modified bentonite supports and immobilized FePc (0.5 wt%) catalyst samples, (solid/monomer ratio = 3.56%, w/w). In most cases, the curves show induction periods up to ~4 h, linked probably with perturbed initiation in absence of initiator or cocatalyst. Much higher polymer yields were produced, as compared with NiPc and CuPc/unmodified bentonite systems at similar conditions, in absence of cocatalyst (viz., only 6.4% for NiPc and 0.0% for CuPc, both of 1.8 wt% at 80 °C [3]). Both pure unmodified bentonite and polycrystalline FePc

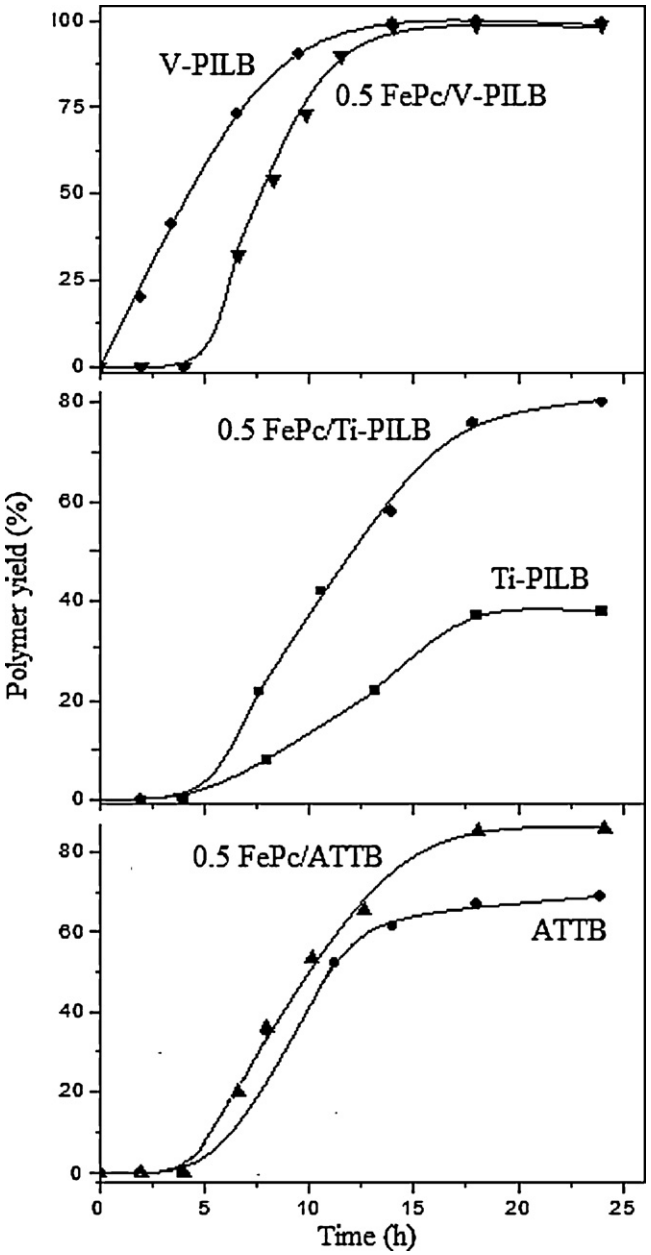

Fig. 8. Kinetic curves of *in situ* polymerization of MMA in presence of modified bentonite supports, ATTB, Ti-PILB and V-PILB and various immobilized FePc (0.5 wt%) samples.

Table 4
Kinetic parameters of *in situ* polymerization of MMA at 60 °C in presence of modified bentonite supports and various immobilized FePc samples.

Samples	k_p ($\times 10^2$ h^{-1})	n_p	$\overline{M}_w$	$\overline{M}_w/\overline{M}_n$	C_T
ATTB	0.66	1.64	392,148	1.80	–
Ti-PILB	2.16	1.16	398,544	4.50	–
V-PILB	285.84	0.56	259,751	3.78	–
FePc/ATTB	30.32	0.77	689,307	1.63	104.80
FePc/Ti-PILB	7.77	1.09	878,844	1.33	440.04
FePc/V-PILB	166.46	0.51	309,586	2.02	0.00

were inactive. Table 4 includes polymerization rate constant (k_p) and reaction order (n_p), calculated by differential analysis of the kinetic curves [50], weight-average molecular weight ($\overline{M}_w$) and polydispersity index ($\overline{M}_w/\overline{M}_n$) of the produced polymers, where $\overline{M}_n$ is number-average molecular weight, and chain transfer constant (C_T), estimated by the aid of modified Mayo equation [51], namely, $1/P_n = 1/P_n^\circ + C_T$ [FePc]/[MMA], where P_n is the number-average degree of polymerization in presence of FePc and P_n° is the number-average degree of polymerization in presence of neat support, i.e., without a chain transfer agent, and concentrations of FePc and MMA are taken in moles g^{-1} reaction mixture. As shown from this table, the reaction follows almost first order kinetics, where k_p values (in h^{-1}) indicate an enhancing role of FePc on polymerization rate, compared to the used supports, particularly ATTB and Ti-PILB. The neat V-PILB, however, possesses the highest activity, due probably to the availability of vanadium redox pairs (viz., V^{4+}/V^{5+} or V^{3+}/V^{4+}), subject to interaction with FePc, together with the clay acid sites. The latter are assumed to take the main part in the polymerization in presence of neat modified bentonite supports.

The C_T values obtained confirm the role of FePc, as a chain transfer agent in the reaction mechanism, being decreased according to the support used in the order, Ti-PILB > ATTB > V-PILB. The same decreasing order is also exhibited by $\overline{M}_w$ and $\overline{M}_n$ (Table 4, from GPC analysis) of PMMA produced by using different immobilized FePc samples, ensuring more contribution of FePc in the polymerization process [13]. Moreover, the polydispersity indices $\overline{M}_w/\overline{M}_n$ approaching ~1, i.e., narrower molecular weight distributions (MWD), for polymers produced by immobilized FePc, compared to neat supports, reveal the regulating role of the complex, encouraged by its facile accessibility in the propagation steps. The chain growth of the polymer produced using FePc/Ti-PILB is exemplified in Fig. 9, through the change in $\overline{M}_w$ and $\overline{M}_n$, as a function of the polymerization duration (2–18 h). A linear evolution of $\overline{M}_n$ with % monomer conversion (Y), fitting an empirical relationship of the type: $\overline{M}_n = AY$ (where constant $A = 8.35 \times 10^3$ a.u.), suggests that the process is well controlled, the initiation is fast

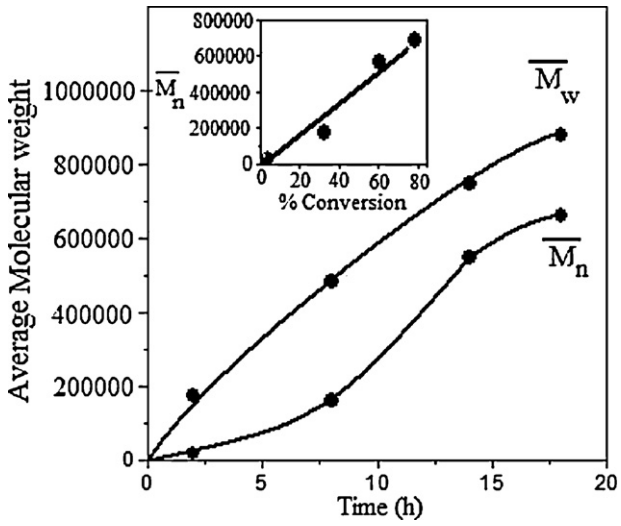

Fig. 9. $\overline{M}_w$ and $\overline{M}_n$ of PMMA produced in presence of FePc/Ti-PILB, as a function of polymerization time. Inset: direct dependence of $\overline{M}_n$ on MMA % conversion.

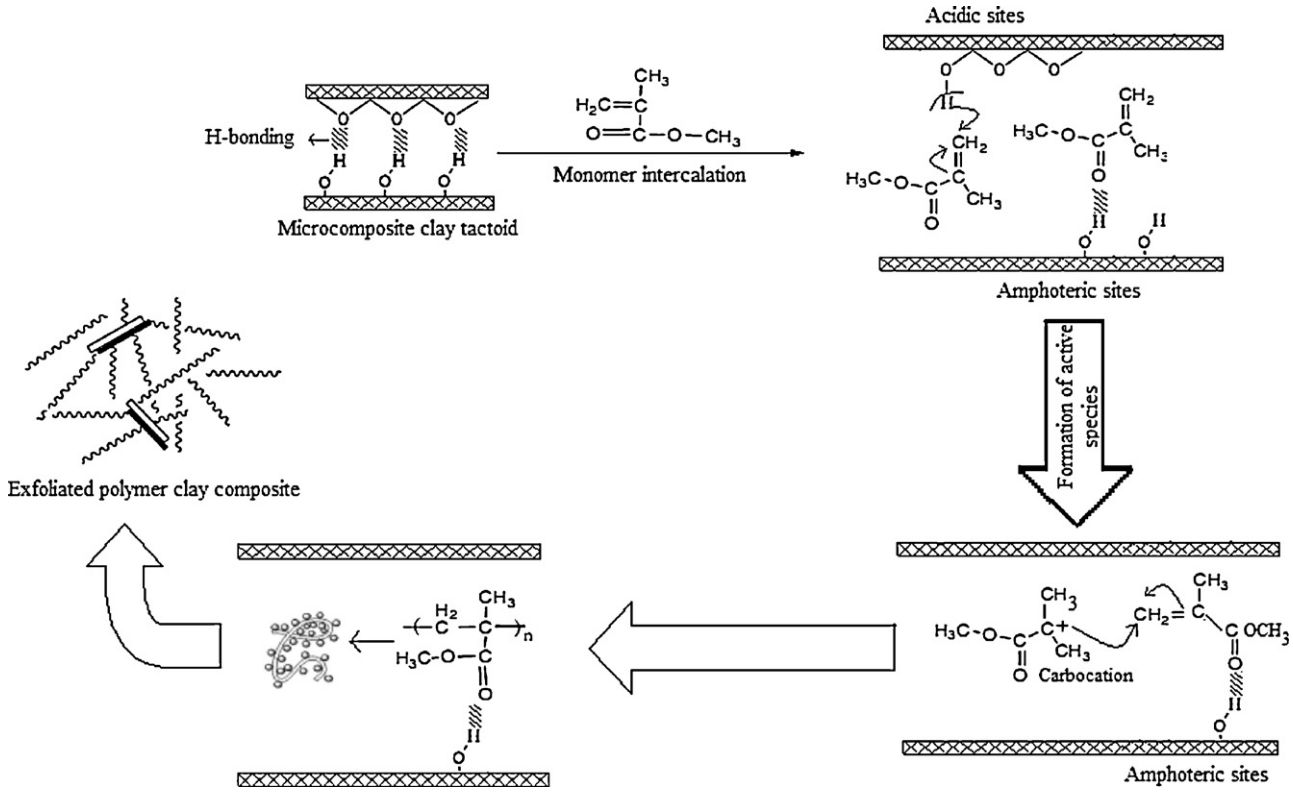

Scheme 1. Proposed reaction pathway of *in situ* polymerization of MMA functioned by various sites existed in the modified bentonite clay galleries.

and the chain breaking events are negligible up to ~75% conversion [3,18].

Based on the obtained results, various polymerization acts taking place in presence of neat modified bentonite samples, as functioned by existed acid sites in the clay galleries, may be represented in Scheme 1. Brønsted acid sites are mainly responsible for the initiation step when attacking the π cloud of the monomer, whereas a complementary role may be displayed by amphoteric sites to organize MMA molecules during the propagation. Through some cationic polymerization, the chain growth can end most likely with formation of exfoliated polymer–clay composite [52]. On the other hand, in contrast to NiPc and CuPc/unmodified bentonite systems, where initiation depended solely on the accessibility (related to orientation modes) of complexes to MMA and bisulfite cocatalyst, in a redox-initiated mechanism [3,18], the role of FePc intercalated in the modified clay galleries, in the present study without cocatalyst, may be described in Scheme 2, as a chain transfer agent, in combination with the acid sites [13]. While the acid sites are fully responsible for the main steps (initiation, propagation and termination), the role of FePc starts in the re-initiation step. Here, the proton axially ligated to FePc can revive the formed dormant species, regenerating thereby the polymer growing chains in the so-called "living polymerization". To confirm living fashion of the polymerization process, within the role of FePc in re-initiation of the dormant polymer, a guide experiment was carried out, where further addition of MMA monomer (2.8 g) to the two catalyst sys-

1- Initiation step

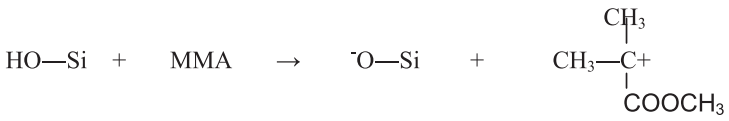

[Brønsted acid sites (OH groups attached to tetrahedral silica)] [Active species (P_1^+)]

2- Propagation steps

$P_1^+ + MMA \rightarrow P_2^+$

$P_2^+ + MMA \rightarrow P_3^+$

$P_3^+ + n\ MMA \rightarrow P_n^+$

[Growing chains]

3- Termination steps

(a) Disproportionation process

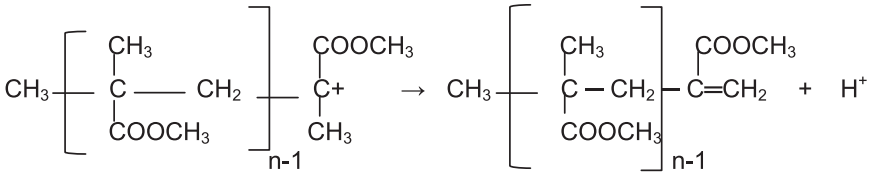

Growing chain PMMA (P_n^+) Terminated chain (Dead chain) [D_n]

(b) Rearrangement process

$P_n^+ + MMA \rightarrow D_n + P_1^+$

(low possibility due to steric hindrance) (Dormant species)

4- Reinitiation step and additional growth of polymeric chains (Catalytic chain transfer mechanism, CCT)

$Fe^{II}Pc + H^+ \rightarrow Fe^{II}Pc \dashrightarrow H^+$ (proton axially ligated to FePc)

$D_n + Fe^{II}Pc \dashrightarrow H^+ \rightarrow P_n^{\bullet} + Fe^{III}Pc$

(Regeneration of polymer growing chain)

$P_n^{\bullet} + m\ MMA \rightarrow P^{\bullet}_{m+n}$

$P^{\bullet}_{(m+n)} + Fe^{III}Pc \rightarrow D_{m+n} + Fe^{II}Pc + H^+$

$MMA + Fe^{II}Pc \dashrightarrow H^+ \rightarrow P_1^{\bullet} + Fe^{III}Pc$

$D_{m+n} + Fe^{II}Pc \dashrightarrow H^+ \rightarrow P^{\bullet}_{m+n} + Fe^{III}Pc$

Scheme 2. Proposed reaction pathway of *in situ* polymerization of MMA in view of combined roles of acidic sites in bentonite clay galleries and intercalated FePc complex molecules.

Table 5
Stereoregularity of PMMA in different PMMA/FePc (0.5 wt%)/modified bentonite composites.

Composite system	Tactospecificity (%)			β 4 [mm]·[rr]/[mr]^2	α 2 [rr]/[mr]
	mm (isotactic)	mr (atactic)	rr (syndiotactic)		
Pure PMMA	17.0	35.5	47.5	2.56	2.68
PMMA/FePc/ATTB	22.2	34.7	43.1	2.65	2.48
PMMA/FePc/V-PILB	5.2	39.6	55.2	0.79	2.79
PMMA/FePc/Ti-PILB	4.5	37.9	57.6	0.72	3.04

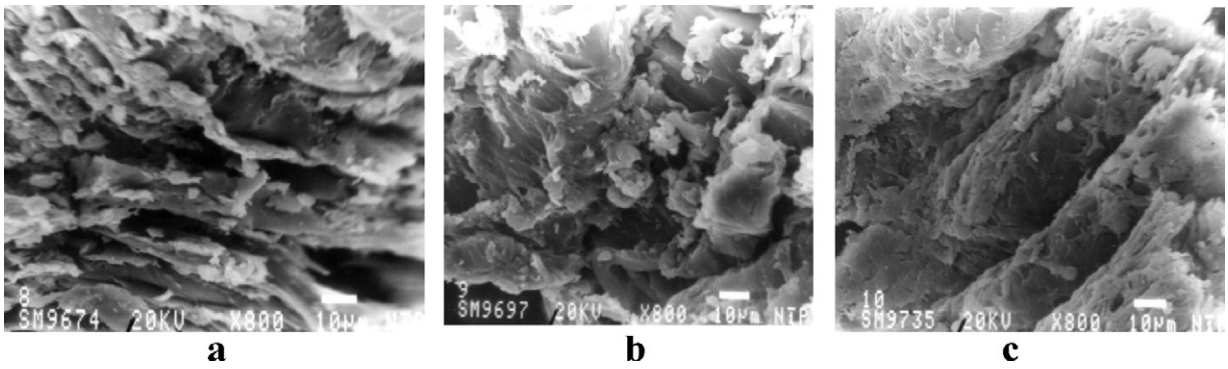

Fig. 10. SEM micrographs of: (a) PMMA/FePc/ATTB, (b) PMMA/FePc/Ti-PILB and (c) PMMA/FePc/V-PILB composites.

tems, viz., FePc/ATTB and FePc/Ti-PILB, after completion of the reaction at 60 °C, led to an increased polymer yield (from 85.6 to 94.4% in case of FePc/ATTB and from 79.9 to 87.5% in case of FePc/Ti-PILB) with increased $\overline{M}_n$ values (from 422,888 to 470,387 in case of FePc/ATTB and from 660,785 to 879,965 in case of FePc/Ti-PILB), exhibiting the same narrow MWDs.

3.5. Polymer/clay composites as in situ polymerization end products

Adopting the *in situ* polymerization of MMA, under the applied conditions, an attempt was made to synthesize polymer–clay composites of promising characteristics as end products. A three component-system was built, consisting of modified bentonite clay, namely, ATTB, Ti-PILB or V-PILB (as filler), oriented FePc complex of 0.5 wt% (as compatibilizer, coupling agent and chain transfer catalyst) and PMMA (as matrix). During *in situ* polymerization, the polymer chains may grow horizontally or vertically in the clay galleries, depending on the functionality of acid sites in the interlayers and on the complex dispersion and orientation, to form either intercalated, partially exfoliated (fully end functionalized) or completely exfoliated (partially end functionalized) composites [52].

The ^{1}HNMR results of stereoregularity, summarized in Table 5, indicate that PMMA in the synthesized composite systems are predominantly syndiotactic. Close data were obtained previously for PMMA produced radically with CCl_4/Ru(II) complex [53], in toluene at 60 °C, namely, rr/mr/mm (syndiotactic/atactic/isotactic) = 53:38:9. This may support the participation of free radicals in polymerization mechanism in the present study. Composites involving V-PILB and Ti-PILB, possess higher degrees of syndiotacticity, compared to pure PMMA and ATTB composite system. Moreover, the calculated β values (=4[mm] [rr]/[mr]^2) [54], for syndiotactic polymers in the two composite systems are close to 1, ensuring the chain-end control mechanism [3,54]. The α values (=2[rr]/[mr]) of the polymers produced in all cases are far from 1, indicating no enantiomorphic site-control approach and confirming that enchainment under the applied conditions is not FePc catalyst-controlled [53,54].

Polymer intercalation/partial exfoliation for all composites could be evidenced by combined FTIR spectra recorded. In these spectra, characteristic frequencies for PMMA (viz., at 2993, 1728 and 1192 cm^{-1}, assigned to C–H, C=O and α-CH_3 stretching, respectively, of isotactic PMMA, and at 1454, 1388 and 1242 cm^{-1} corresponding to δ CH_2, α-CH_3 and C–O stretching, respectively, of syndiotactic PMMA [55,56]), could be observed together with those of modified bentonite, namely, at 3400–3600 cm^{-1}, 980–1050 cm^{-1}, 610 cm^{-1} and 469 cm^{-1}, assigned to O–H stretching of lattice water, Si–O stretching, coupled Al–O and Si–O out of plane and Si–O–Si bending, respectively [41,45].

The morphology of various composites under study is illustrated in Fig. 10. Clay granules are shown clearly dispersed in PMMA matrix, with an average size of ~1875 nm and 25 nm in composites involving ATTB and V-PILB, respectively (micrographs a and b). They are fixed as fillers in the polymeric matrix, resulting in some ordered PMMA-layered structure. The *nano-sized* PMMA-VPILB composite may be formed in an enhanced polymerization, through interaction of FePc compatibilizer with V-pillar, causing its dissociation and even dispersion in the composite system. The modified clay layers seem partially exfoliating on the PMMA base, with some larger intercalated tactoids. In Ti-PILB *micro-composite*, larger particles (ranged between 5000 and 6600 nm) are seen to be unevenly distributed, with hollow and clay flowery shapes (micrograph c), probably poorly attached to PMMA matrix. Further investigations into detailed characteristics of the obtained composites will be the subject of a forthcoming article.

4. Conclusion

The hybrid catalytic systems under study consisted of iron phthalocyanine (FePc, 0.5 wt%) immobilized on modified bentonite supports (acid/thermally treated, ATTB, vanadia-pillared, V-PILB and titania-pillared, Ti-PILB). The applied characterization techniques confirmed that FePc causes reorientation of the clay layers in all cases, with more stacking order. FePc was incorporated into the clay galleries, in a pronounced accessibility favored by inclined edge-on interaction between *N*'s of the macro-ring system and the edge OH sites of the clay, via asymmetric Brønsted interaction. Strong interaction of FePc with vanadia pillar, located near the layer edges, led to its dissociation into nano-sized isolated tetrahedral species (12–19 nm) of higher Lewis acidity, impeding

the vanadia–intelayer sites interaction. In FePc/Ti-PILB, where titania existed in flocculated form (88 nm), weakly interacted with silica tetrahedral sheets, FePc seemed to interact preferentially with the interlayer and edge sites, rather than with titania pillar. Through application of these catalytic systems in the *in situ* polymerization of MMA, Brønsted acid sites of modified bentonite supports were responsible for the initiation step, while amphoteric sites contributed in organizing chains produced during the propagation. In contrast to NiPc and CuPc systems, where initiation depended on accessibility of complexes to MMA and bisulfite cocatalyst in a redox-initiated mechanism, FePc could involve as a chain transfer agent in the re-initiation step, reviving the dormant species in a living polymerization. Its regulating role was encouraged by the accessible oriented profile. The polymerization end products were studied *in situ* with the used hybrid catalytic systems. Partial exfoliation (through fully end functionalization) was evident, particularly in PMMA/FePc/V-PILB composite, where nano-clay particles of 25 nm existed, with more ordered polymer chains and well dispersed vanadia pillar species, in a strong interaction and high compatibility with FePc.

References

[1] B.B. Wayland, G. Poszmik, S.L. Mukerjee, J. Am. Chem. Soc. 116 (1996) 7943.
[2] F. Ueda, M. Matsuyama, M. Kamigaito, M. Sawamoto, Macromolecules 31 (1998) 557.
[3] E.M. Sadek, M.A. Mekewi, F.Z. Yehia, S.M. Solyman, S.A. Hassan, Macromol. Chem. Phys. 202 (2001) 1505.
[4] M.R. Nabid, R. Sedghi, P.R. Jamaat, N. Safari, A.A. Entezami, Appl. Catal. A 328 (2007) 52.
[5] Y.I. Yermakov, N. Kuznetsov, V.A. Zakharov, Catalysis by Supported Complexes, Elsevier Sci. Publ. Comp., New York, 1981.
[6] S.A. Hassan, S.A. Sadek, S.M. Faramawy, M.A. Mekewi, Stud. Surf. Sci. Catal. 100 (1996) 407.
[7] S.A. Hassan, A.A. Zahran, F.Z. Yehia, Adsorption Sci. Technol. 20 (2002) 269.
[8] J.S. Yadav, B.V.S. Reddy, G. Satheesh, Tetrahedron Lett. 45 (2004) 3673.
[9] S. Lu, E. Ruth, I.R. Kaplan, Org. Geochem. 14 (1989) 491.
[10] S.A. Hassan, A.M. Mousa, M. Abdel Khalik, A.A. Abdel Azim, J. Catal. 53 (1978) 175.
[11] A.A. Harrane, N. Naar, M. Belbachir, Mater. Lett. 61 (1978) 3555.
[12] H. Datta, N.K. Singha, A.K. Bhowmick, Macromolecules 41 (2008) 50.
[13] H. Akat, M.A. Tasdelen, F. Du Prez, Y. Yagci, Eur. Polym. J. 44 (2008) 1949.
[14] T. Agag, T. Takeichi, Polymer 41 (2006) 7083.
[15] Z. Qian, G. Hu, S. Zhang, M. Yang, Phys. B: Conden. Matter 403 (2008) 3231.
[16] Y. Li, B. Zhang, Pan S X., Compos. Sci. Technol. 68 (2008) 1954.
[17] J. Arfaoui, L.K. Boudali, A. Ghorbel, Catal. Commun. 7 (2006) 86.
[18] S.A. Hassan, F.Z. Yehia, A.A. Hamed, A.A. Zahran, S.M. Solyman, J. Porous Mater., doi:10.1007/s10934-009-9350-z, 2010.
[19] A. Gil, H.L. Del Castillo, J. Masson, J. Court, P. Grange, J. Mol. Catal. A: Chem. 107 (1996) 185.
[20] T. Kaneko, M. Fujii, T. Kodama, Y. Kitayama, J. Porous Mater. 8 (2001) 99.
[21] N.N. Binitha, S. Sugunan, Micropor. Mesopor. Mater. 93 (2006) 82.
[22] N. Jagtap, V. Ramaswamy, Appl. Clay Sci. 33 (2006) 89.
[23] K.L. Boudali, A. Ghorbel, P. Grange, Appl. Catal. A 305 (2006) 7.
[24] K.L. Boudali, A. Ghorbel, P. Grange, F. Figueras, Appl. Catal. B 59 (2005) 105.
[25] J. Khedher, A. Ghorbel, Stud. Surf. Sci. Catal. 130 (2000) 1649.
[26] M.A. Vicente, J.F. Lambert, Phys. Chem. Chem. Phys. 3 (2001) 4843.
[27] F.J. Anaissi, G.J.F. Demets, H.E. Toma, S. Dovidauskas, A.C.V. Coelho, Mater. Res. Bull. 36 (2001) 289.
[28] S.A. Hassan, H.A. Hassan, K.M. Hashem, H.M. Abdel Dayem, Appl. Catal. A 300 (2006) 14.
[29] H. Kameyama, F. Narumi, T. Hattori, H. Kameyama, J. Mol. Catal. A: Chem. 258 (2006) 172.
[30] A.M. Machado, F. Wypych, S.M. Drechsel, S. Nagaki, J. Colloid Interface Sci. 254 (2002) 158.
[31] M.S.M. Moriera, P.R. Martins, R.B. Curi, O.R. Nascimento, Y. Iamamoto, J. Mol. Catal. A: Chem. 233 (2005) 73.
[32] E.P. Giannelis, Adv. Mater. 8 (1996) 29.
[33] I.K. Biernacka, A.R. Silva, A.P. Carvalho, J. Pires, C. Freire, J. Mol. Catal. A: Chem. 278 (2007) 82.
[34] F.H. Moser, A.L. Thomas, Phthalocyanine Compounds, Rienhold Publishing Corp., New York, 1963.
[35] S.S. Gupta, K.G. Bhattacharyya, J. Colloid Interface Sci. 295 (2006) 21.
[36] H. Kita, N. Henmi, K. Shimazu, H. Hattori, J. Tanabe, J. Chem. Soc. Faraday Trans. 77 (1981) 2451.
[37] X. Yang, Z. Sun, D. Wang, W. Forsling, J. Colloid Interface Sci. 293 (2007) 47.
[38] K.S.W. Sing, D.H. Everret, R.A.W. Haul, L. Moscou, R.A. Pierotti, J. Rouquerol, T. Siemieniewska, IUPAC, Pure Appl. Chem. 57 (1985) 603.
[39] G.E. Christidis, P.W. Scott, A.C. Dunham, Appl. Clay Sci. 12 (1997) 329.
[40] M. Lenarda, L. Storato, G. Pellegrini, L. Piovesan, R. Grnzerla, J. Mol. Catal. A: Chem. 145 (1999) 237.
[41] E. Eren, B. Afsin, Y. Onal, J. Hazard. Mater. 149 (2008) 59.
[42] L. Chmielarz, P. Kustrowski, M. Zbroja, A.R. Lasocha, B. Dudek, R. Dziembaj, Appl. Catal. B 45 (2003) 103.
[43] B.D. Cullity, Elements of X-ray Diffraction, Addison–Wesley Publishing Co. Inc., 1976, Chapter 14.
[44] F. Ayari, E. Srasra, M.T. Ayadi, Desalination 185 (2005) 391.
[45] M. Kurian, S. Sugunan, Micropor. Mesopor. Mater. 83 (2005) 25.
[46] J. Madejová, Vib. Spectrosc. 31 (2003) 1.
[47] P. Kuśtrowski, Y. Segura, L. Chmielarz, J. Surman, R. Dziembaj, P. Cool, E.F. Vansant, Catal. Today 114 (2006) 307.
[48] P. Zarzycki, F. Thomas, J. Colloid Interface Sci. 302 (2006) 547.
[49] O. Touret, C.H. Pons, D. Tessier, Y. Tardy, Clay Miner. 25 (1990) 217.
[50] H.M. AbdelDayem, H.A. Hassan, S.A. Hassan, J. Dispersion Sci. Technol. 28 (2007) 892.
[51] S.C.J. Pierik, A.M. van Herk, J. Appl. Polym. Sci. 91 (2004) 1375.
[52] X. Wang, F. Tao, G. Xue, J. Zhu, T. Chen, P. Sun, H.H. Winter, A.C. Shi, Macromol. Mater. Eng. 294 (2009) 190.
[53] M. Kato, M. Kamigaito, M. Sawamoto, T. Higashimura, Macromolecules 28 (1995) 1721.
[54] Y. Nakayama, T. Shibahara, H. Fukumoto, A. Nakamura, Macromolecules 29 (1996) 8014.
[55] G. Pistoia, M.A. Voso, J. Polym. Sci. Part A: Polym. Chem. 14 (1976) 1811.
[56] R. Zbindin, Infrared Spectroscopy of High Polymers, Academic Press, New York, 1964.